CO Adsorption on a Mixed-Valence Ruthenium Metal–Organic Framework Studied by UHV-FTIR Spectroscopy and DFT Calculations

ARTICLE *in* THE JOURNAL OF PHYSICAL CHEMISTRY C · FEBRUARY 2013

Impact Factor: 4.77 · DOI: 10.1021/jp3056366

THE JOURNAL OF PHYSICAL CHEMISTRY C

Article

pubs.acs.org/JPCC

CO Adsorption on a Mixed-Valence Ruthenium Metal–Organic Framework Studied by UHV-FTIR Spectroscopy and DFT Calculations

Heshmat Noei,[†,+] Olesia Kozachuk,[‡] Saeed Amirjalayer,[‡] Sareeya Bureekaew,[‡] Max Kauer,[§] Rochus Schmid,*[,‡] Bernd Marler,[⊥] Martin Muhler,[†] Roland A. Fischer,*[,‡] and Yuemin Wang*[,†,§]

[†]Laboratory of Industrial Chemistry, [‡]Chair of Inorganic Chemistry II, [§]Chair of Physical Chemistry I, and [⊥]Institute of Geology, Mineralogy and Geophysics, Ruhr-University Bochum, Universitaetsstrasse 150, 44780 Bochum, Germany

ABSTRACT: The mixed-valence metal–organic framework $[Ru_3^{II,III}(btc)_2Cl_{1.5}]$ (**Ru-MOF**) was synthesized by the controlled SBU approach and characterized by combined powder XRD, XPS, and FTIR methods. The interaction of CO molecules with **Ru-MOF** was studied by a novel instrumentation for ultra-high-vacuum (UHV) FTIR spectroscopy. The high-quality IR data demonstrate the presence of two different CO species within the framework: a strongly bonded CO showing a low-lying band at 2137 cm^{-1} and a second CO species at 2171 cm^{-1} with a lower binding energy. It was found that these IR bands cannot be assigned in a straightforward manner to CO molecules adsorbed on the coordinatively unsaturated Ru^{II} site (CUS) and Ru^{III} site connected to an additional Cl^- ion for charge compensation. The accurate DFT calculations reveal that the structural and electronic properties of the mixed-valence **Ru-MOF** are much more complex than expected. One of the Cl^- counterions could be transferred to a neighboring paddle-wheel, forming an anionic SBU blocked by two Cl^- counterions, whereas the other positively charged paddle-wheel with a $Ru_2^{II,III}$ dimer exposes two "free" CUS, which can bind two CO molecules with different frequencies and binding energies.

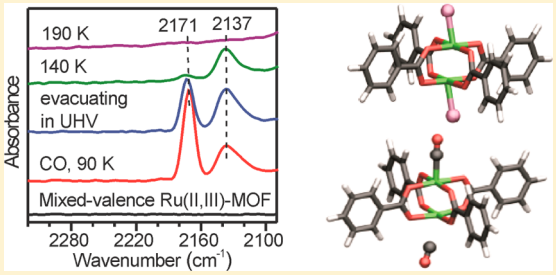

INTRODUCTION

Metal–organic frameworks (MOFs) are relatively new and an intriguing class of crystalline porous materials that can be readily formed by self-assembly of organic (multitopic linkers) and inorganic moieties (metal ions or clusters) via coordination bonds.[1,2] The hybrid nature of these compounds and the rich libraries of available organic linkers and metal ions/clusters create virtually a myriad of combinations for the synthesis of new MOFs. Moreover, the possibility for postsynthetic modification provides an additional dimension to the synthetic variability.[3,4]

To date, a significant progress has been already achieved toward synthesis of highly porous MOFs with various pore metrics and topologies that showed also encouraging results for many application areas ranging from gas storage/separation[5] and sensing[6] over heterogeneous catalysis[7,8] to drug delivery.[9,10] The majority of the developed and well-investigated MOFs are relatively "simple" and presented mainly by single-linker and/or monometallic systems that include separate or clustered metal ions of only one type and charge. However, more "complex" systems formed by integration of various linkers/metals[11] or mixed-valence metal species[12−18] into the building units of the given framework are highly interesting for improving or introducing novel functionalities. In particular, mixed-valence MOFs and/or MOF-composites with induced mixed-valence metal species (for instance, stabilized by guest molecules) demonstrated redox-activity[12,18] and electric conducting properties[19,20] that are important to be applicable to a porous electrode for batteries, fuel cells, capacitors, etc. Moreover, mixed-valence in MOFs may be also the origin of interesting magnetic effects. Despite intensive progress in designing and synthesis, the incorporation of mixed-valence species into a single MOF structure remains a challenge, and a number of stable highly porous frameworks that contain identical metal ions in two distinct oxidation states are rather limited.

On the basis of the previous IR studies on $[Cu_3(btc)_2]$,[21] in this contribution, we present our developed studies on mixed-valence ruthenium(II,III) (abbreviated in the following text as "**Ru-MOF**")[22] analogue of HKUST-1.[23] HKUST-1 MOF is based on square paddle-wheel carboxylate copper units that act in the coordination polymer construction as 4-connected nodes together with 3-connected anionic linkers btc^{3-} (benzene-1,3,5-tricarboxylate) to build $[Cu_3(btc)_2]$.[23] In general, the paddle-wheel unit is a well-known molecular compound type in coordination chemistry for various metals, and therefore, it is an often choice for the designing of MOFs as well.[24] Regarding the HKUST-1 structural type, in particular, being first reported for copper, an isostructural MOF of the $[M_3(btc)_2]$ composition that incorporates Mo,[25] Cr,[26] or Zn[27] was also achieved. A peculiar feature of guest-free $[M_3(btc)_2]$ structures is the presence of accessible, open metal sites at axial positions of paddle-wheel units. These coordinatively unsaturated sites (CUS), which are distributed within the frameworks in a

Received: June 8, 2012
Revised: February 26, 2013
Published: February 26, 2013

repeating, regular fashion, have been shown to be important for catalytic activity and can enhance the general adsorption properties of the materials, due to the partial positive charges on the metal centers.[7] As follows, an interesting structural type and a possibility to modulate metal type have motivated us to prepare HKUST-1 analogues with the metals that readily form both homo- and heterovalent paddle-wheel units.

Recently, we have succeeded in the synthesis of ruthenium MOF of HKUST-1 structure.[22] In contrast to all other known $[M_3(btc)_2]$ frameworks that are based on $M_2^{II,II}$ units, we showed that mixed-valence $M_2^{II,III}$ paddle-wheels units, as the most stable ones known for ruthenium, are formed in **Ru-MOF**. Hence, preserving the general HKUST-1 structure, **Ru-MOF**, $[Ru_3^{II,III}(btc)_2Cl_{1.5}]$, is a more complex, but stable, system of mixed-valence nature with two different metal centers and additional counterions, Cl^- (or, in general, other X^-, such as OH^-), to compensate the charge of the framework. Thus, the question about potential active metal sites and reactivity of such MOFs is not trivial (and certainly differ from known $[M_3(btc)_2]$ systems) and an accurate probing of the local metal environment is highly important and necessary on this type of materials.

In this work, we investigate the adsorption of CO on **Ru-MOF** employing a novel ultra-high-vacuum (UHV) FTIR spectroscopy[28] in conjunction with density functional theory (DFT) calculations. The IR data obtained by applying small probe molecules, such as CO and CO_2, are expected to provide important information about electronic and structural properties of the local metal environment,[29,30] as demonstrated by our recent study on Cu-based MOFs (HKUST-1 and MOF-14)[21] and ZnO@ZIF-8.[31] Here, we present high-quality IR data that allow us to gain detailed insight into the adsorption of CO on **Ru-MOF**. On the basis of the accurate theoretical calculations, we demonstrate that the interaction of CO with mixed-valence **Ru-MOF** is of a complex nature and the IR bands cannot be assigned in a straightforward manner as is usually done and reported for other mixed-valence MOFs.[13] The calculations suggest the possibility that a Cl^- counterion could be transferred to a neighboring paddle-wheel unit, resulting in a charge separation and alternating cationic and anionic Ru_2 dimers. Whereas the negatively charged dimer is fully coordinated to Cl^- ions, the cationic $Ru_2^{II,III}$ dimer possesses two CUS, where two different adsorbed CO species can be formed, as supported by the IR data.

EXPERIMENTAL AND COMPUTATIONAL DETAILS

Synthesis of $[Ru_3^{II,III}(btc)_2Cl_{1.5}]$ (Ru-MOF).[22] A mixture of $[Ru_2(OOCCH_3)_4Cl]$ (170 mg, 0.36 mmol), H_3btc (101 mg, 0.48 mmol), CH_3COOH (0.7 mL), and H_2O (4 mL) was heated at 160 °C for 24 h in a Teflon-lined autoclave. After cooling to room temperature, a deep green product was collected with a membrane filter, washed with water, and dried at room temperature. The activation of the resulting product was conducted by heating at 150 °C under a dynamic vacuum (ca. 10^{-3} mbar) for 24 h. All chemicals and solvents were purchased from commercial suppliers and used without further purification. Before further manipulations, activated **Ru-MOF** samples were stored under an inert gas atmosphere in a glovebox. $[Ru_2(OOCCH_3)_4Cl]$ was prepared by using a procedure previously described.[32]

Instrumental. X-ray photoelectron spectroscopy (XPS) measurements were carried out in a UHV setup equipped with a high-resolution Gammadata-Scienta SES 2002 analyzer. A monochromatic Al Kα X-ray source (energy 1486.6 eV) was used as incident radiation. The analyzer slit width was set at 0.3 mm and the pass energy was fixed at 200 eV for all the measurements. The overall energy resolution was better than 0.5 eV. A flood gun was used to compensate for the charging effects. All spectra reported here are calibrated to the C 1s core-level binding energy at 285 eV. The XP spectra were deconvoluted using the CASA XPS program with a mixed Gaussian−Lorentzian function and Shirley background subtraction. Powder X-ray diffraction (PXRD) measurements of the sample were recorded on a D8-Advance Bruker AXS diffractometer with Cu Kα radiation (λ = 1.5418 Å) and a focused Göbel mirror in $\theta-2\theta$ geometry with a position-sensitive detector in a 2θ range from 5 to 90° at a scan speed of 10 s per step. The instrumental setup was in capillary mode. The sample was filled under inert gas (glovebox) into capillaries that were then flame-sealed prior to the measurement. Far-IR spectra were recorded using a Nicolet 6700 FTIR spectrometer in the ATR geometry with a diamond ATR unit. The spectra were collected with 32 scans at a resolution of 4 cm^{-1}. UHV-FTIR experiments were performed by using a state-of-the-art vacuum IR spectrometer (Bruker, VERTEX 80v) coupled to a novel UHV system (Prevac, for details, see ref 28). The base pressure in the measurement chamber was 2×10^{-10} mbar. The optical path inside the IR spectrometer and the space between the spectrometer and UHV chamber were evacuated to avoid atmospheric moisture adsorption, resulting in a superior sensitivity and stability of the system. For the UHV-FTIRS measurements, the **Ru-MOF** powder sample was first pressed onto a gold-plated stainless-steel grid and then mounted on a sample holder that was specially designed for the FTIR transmission measurements under UHV conditions. Prior to each exposure, a spectrum of the clean **Ru-MOF** sample was recorded to be used as a background reference. We carried out the exposure of the sample to CO by backfilling the measurement chamber through a leak valve. All UHV-FTIR spectra were collected with 1024 scans at a resolution of 4 cm^{-1} in transmission mode.

DFT Calculations. All theoretical calculations have been performed for nonperiodic model systems of a single paddle-wheel building block, using the TURBOMOLE (V6.3)[33] suite of programs. The systems have been optimized with density functional theory (DFT) using the B3LYP hybrid functional[34−37] and cc-pVDZ basis sets (for ruthenium, the corresponding cc-pVDZ-PP valence basis set with an effective core potential was employed).[38,39] In addition, D3 dispersion corrections according to Grimme et al.[40] were added to the energy expression, throughout. This well-established level of theory was chosen in particular for consistency with our first-principles derived force field, MOF-FF, where it is used for the reference calculations.[41] At stationary points, analytic second derivatives were computed with the AOFORCE program. In all calculations, a finer grid (m5) was used in order to improve especially the low vibrational modes. In addition to unscaled vibrational normal modes, we also scaled the modes by a factor of 0.9745, which was calibrated in order to reproduce the experimental gas phase stretching frequency of CO (2143 cm^{-1}).[42] Because of the expected large ligand field splitting of ruthenium, all systems were computed in its low-spin configuration, using an unrestricted open shell calculation.

dx.doi.org/10.1021/jp3056366 | J. Phys. Chem. C 2013, 117, 5658−5666

RESULTS AND DISCUSSION

Synthesis and Characterization of $[Ru_3^{II,III}(btc)_2Cl_{1.5}]$ (Ru-MOF). As we reported previously,[22] the ruthenium structural analogue of HKUST-1 was first prepared using the reaction of ruthenium(III) chloride with 1,3,5-benzenetricarboxylic acid in water/acetic acid solution under solvothermal conditions (160 °C for 72 h, Teflon-lined autoclave). In this paper, we have rationalized the synthesis of the **Ru-MOF** by applying the so-called "controlled SBU (secondary building unit) approach" that implies the direct use of the preformed SBU precursors of needed geometry.[43,44] In the HKUST-1 structural type, the paddle-wheel metal clusters could be considered as SBUs that define MOF architecture. Thereby, for **Ru-MOF** preparation, taking into account also the revealed mixed-valence $Ru_2^{II,III}$ state,[22] a $[Ru_2^{II,III}(OOCCH_3)_4Cl]$ complex was selected as a SBU precursor. The structure of this polymeric compound is arranged by $\{Ru_2(OOCCH_3)_4\}$ paddle-wheel moieties that combined via Cl^- in a 1D zigzag polymer (Figure 1).[32,43−45] The compound is quite stable and

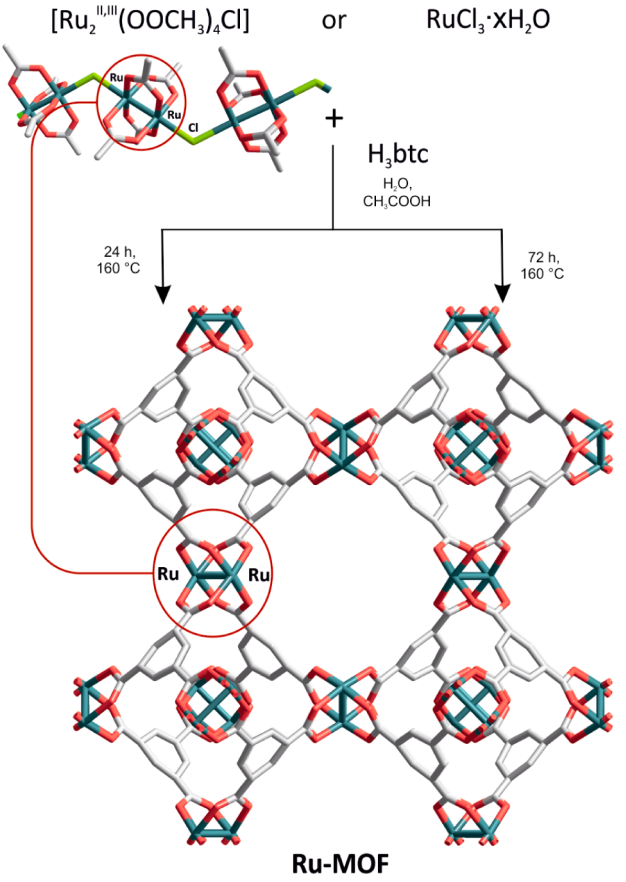

Figure 1. Synthesis and structure of **Ru-MOF**. The H and Cl atoms of the framework are not shown. Each $Ru_2^{II,III}$ paddle-wheel unit in **Ru-MOF** may carry one Cl^- at one axial site; other distributions of Cl^- over CUS at Ru(II,III) are possible (see the discussion below).[22]

is often used as a precursor for the synthesis of ruthenium paddle-wheel-based coordination compounds of various structures and dimensionalities.[46]

Figure 2 shows the powder X-ray diffraction (PXRD) pattern of **Ru-MOF** synthesized by the controlled SBU approach (curve B). The corresponding 2θ values are in a good accord with the data we reported for the sample prepared from $RuCl_3$

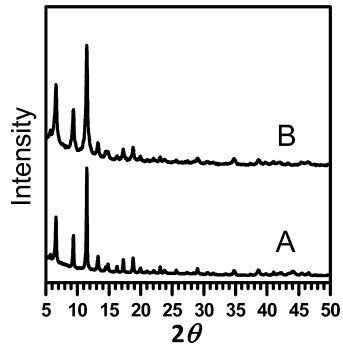

Figure 2. Comparison of PXRD patterns of activated **Ru-MOF** samples prepared: (A) from $RuCl_3{\cdot}xH_2O$ and (B) via the SBU approach, using $[Ru_2^{II,III}(OOCCH_3)_4Cl]$.

(curve A),[22] confirming retention of crystallinity. In addition, N_2 adsorption data of the fully desolvated **Ru-MOF** form collected at 77 K reveal a type I isotherm, which is characteristic of highly microporous materials. The calculated BET surface area amounts to 723.4 $m^2\ g^{-1}$, also in excellent agreement with the value we reported previously for **Ru-MOF** prepared from $RuCl_3$ (704.0 $m^2\ g^{-1}$).[22]

The oxidation state of Ru cations was elucidated by XPS studies. As shown in Figure 3, ruthenium-, oxygen-, chlorine-,

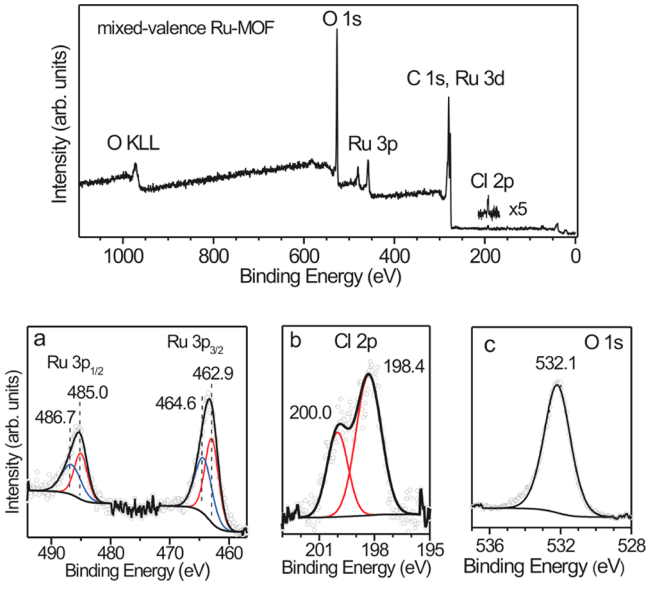

Figure 3. Survey scan of XP spectra of **Ru-MOF** (top) and deconvoluted XP spectra of **Ru-MOF** (bottom): (a) Ru 3p region, (b) Cl 2p region, (c) O 1s region.

and carbon-related peaks are detected in the XP survey spectra obtained for the **Ru-MOF** sample. The Ru 3p peaks in the XP spectrum are dominated by two spin−orbit components of Ru $3p_{3/2}$ and Ru $3p_{1/2}$ (Figure 3a). After deconvolution, two doublets are clearly resolved at 462.9 and 485 eV as well as at 464.6 and 486.7 eV, which are assigned to the Ru^{II} and Ru^{III} species, respectively.[47,48] On the basis of quantitative analysis, the concentration ratio of Ru^{II} to Ru^{III} was estimated to amount to about 1:1. An additional Cl^- counterion is present for charge balance, presumably coordinated to the Ru^{III} site. Expectedly, two peaks are clearly seen at 198.4 and 200 eV resulting from the Cl $2p_{3/2}$ and Cl $2p_{1/2}$ core levels of Cl^-, respectively (Figure

dx.doi.org/10.1021/jp3056366 | J. Phys. Chem. C 2013, 117, 5658−5666

3b).[47] The **Ru-MOF** structure was further characterized by the intense hydrocarbon C 1s peak at 285.0 eV and the carboxylate (−COO) C 1s peak at 288.5 eV. The existence of carboxylate species is also demonstrated by the O 1s peak at 532.1 eV being the only feature detected in the O 1s spectrum (Figure 3c). Importantly, on the basis of the O 1s data, the presence of any oxide impurities is ruled out. Overall, the present XPS results are in good agreement with those obtained for **Ru-MOF** prepared from $RuCl_3{\cdot}xH_2O$.[22]

Hence, the exploitation of the SBU approach by using $[Ru_2(OOCCH_3)_4Cl]$ instead of $RuCl_3$ as a metal source afforded **Ru-MOF** with a considerably decreased reaction time and improvement in the yield of the final product. However, adding acetic acid is necessary to facilitate the exchange of carboxylate linkers. The reaction between $[Ru_2(OOCCH_3)_4Cl]$ and H_3btc without acetic acid only in water at 160 °C provided a mixture of desired MOF and nonreacted precursor even after 72 h, which was difficult to work up.

To consider the composition and structure of **Ru-MOF**, the question about location of the counterion arises. At this point, it is interesting to note that the homologous mixed-valence iron framework, $[Fe_3^{II,III}(btc)_2Cl_{1.5}]$, was previously achieved.[49] It was shown that the chloride counterions in this structure are not coordinated, but disordered inside the pores occupying the large volume together with the solvent DMF (*N*,*N*-dimethylformamide) molecules. For $Ru_2^{II,III}$ paddle-wheel carboxylate compounds with Cl^- acting as counterions, however, an opposite trend has been observed in the literature. Cl^- is tending rather to coordinate to ruthenium centers in both monodentate and bidentate (as bridging ligand) modes, thus, creating polymeric architectures.[50−54] Taking into account the charge balance and structural features of used precursor and **Ru-MOF**, the Cl^- ions are likely occupying one of the axial positions at each paddle-wheel unit. While single-crystal XRD data of **Ru-MOF** was missing, far-IR spectroscopy was used to detect the Ru−Cl bond in **Ru-MOF**. The IR spectrum (Figure 4) shows a band at 303 cm^{-1} assigned to the Ru−Cl stretching

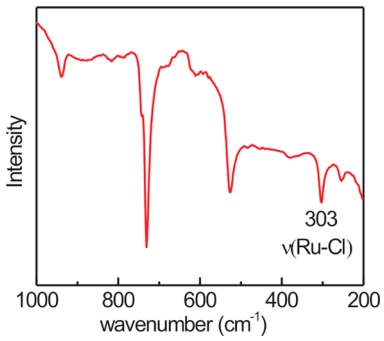

Figure 4. Far-IR spectrum of the mixed-valence **Ru-MOF**. Prior to the IR measurement, the sample was activated by heating under dynamic vacuum (ca. 10^{-3} mbar) at 150 °C for 24 h to remove all incorporated guest molecules.

vibration, in accordance with the literature data.[55] Thereby, in contrast to the $[M_3(btc)_2]$ (Mo,[25] Cr,[26] Fe,[49] or Zn[27]) frameworks, overall, only one empty axial position could be exposed in the activated **Ru-MOF** material, whereas the second site is rather occupied by the counterion.

CO Adsorption on Ru-MOF. To gain more insight into the structural and electronic properties of different ruthenium centers in **Ru-MOF**, we carried out UHV-FTIRS experiments of CO adsorption at temperatures as low as 90 K. The activated **Ru-MOF** powder sample was additionally heated to 450 K in a UHV chamber and then cooled down to 90 K to remove all adsorbed species. The corresponding IR spectra (not shown) reveal that the structure of **Ru-MOF** remains unchanged during thermal treatment. Under UHV conditions with a base pressure of 2×10^{-10} mbar, the adsorption of CO, CO_2, H_2O, or other molecular species from the residual background was found to be negligible on the time scales of the experiments. The availability of a clean and adsorbate-free **Ru-MOF** sample is demonstrated by the absence of any vibrational bands in the concerned IR regions (Figure 5, spectrum A).

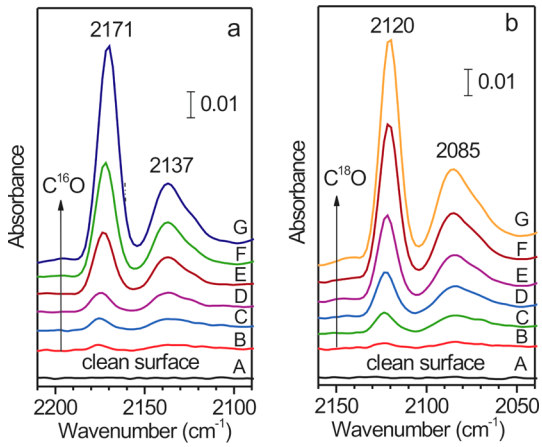

Figure 5. Adsorption of CO at **Ru-MOF**. UHV-FTIR spectra obtained after exposing the clean **Ru-MOF** to (a) $C^{16}O$ and (b) $C^{18}O$ at 90 K. (A) Clean sample; dosing $C^{16}O/C^{18}O$ at 90 K: (B) 5×10^{-7}, (C) 1×10^{-6}, (D) 1×10^{-5}, (E) 5×10^{-5}, (F) 1×10^{-4}, and (G) 5×10^{-4} mbar.

Exposing the clean, activated **Ru-MOF** sample to CO at 90 K led to the appearance of two IR bands at 2171 and 2137 cm^{-1} (Figure 5a), which are assigned to the internal C−O stretch modes. To unambiguously identify the CO-related bands, we performed additional experiments with the $C^{18}O$ isotopomer (Figure 5b). After the $C^{18}O$ exposure at 90 K, two IR bands showed up at 2120 and 2085 cm^{-1} exhibiting the expected isotopic shift with respect to the results recorded for $C^{16}O$. The CO band at 2171 cm^{-1} shifts to higher frequency by 38 cm^{-1} with respect to the gas-phase value (2143 cm^{-1}). In contrast, the 2137 cm^{-1} band shifts slightly to lower frequency compared to the free CO band.

Interestingly, the 2171 cm^{-1} band has already started to decrease in intensity upon evacuation to 10^{-10} mbar after CO exposure at 90 K, while the second band at 2137 cm^{-1} remains unchanged (Figure 6), indicating the presence of two CO species with different binding energies. This finding is further supported by the detailed temperature-dependent FTIR experiments, which provide direct spectroscopic evidence of the thermal stability of different adsorbed CO species. As shown in Figure 7, when annealing to higher temperatures, the IR band at 2171 cm^{-1} shows a rapid decrease in intensity and is removed completely around 150 K while the 2137 cm^{-1} band is more stable and disappears at 190 K, revealing a higher binding energy of the latter CO species.

It is known that the adsorption of CO on metal cations can occur via electrostatic interaction, resulting in a blue shift of the CO stretch frequency with respect to the gas-phase value due

dx.doi.org/10.1021/jp3056366 | J. Phys. Chem. C 2013, 117, 5658−5666

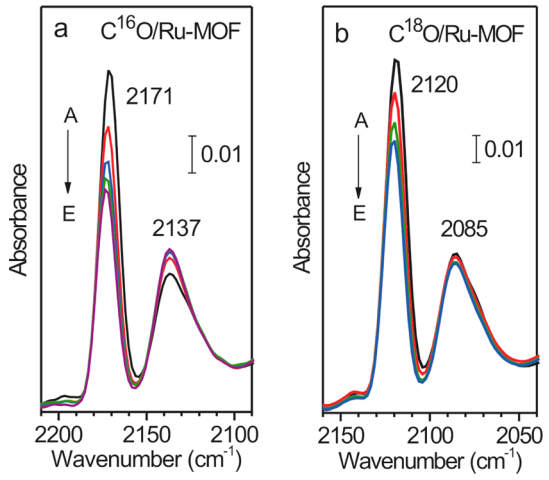

Figure 6. Adsorption and desorption of CO at **Ru-MOF** at 90 K. UHV-FTIR spectra obtained after exposing the clean **Ru-MOF** to (a) $C^{16}O$ and (b) $C^{18}O$. (A) Exposure to $C^{16}O/C^{18}O$ (5×10^{-4} mbar) at 90 K; and then evacuated in UHV (10^{-10} mbar) for (B) 10, (C) 20, (D) 30, and (E) 40 min.

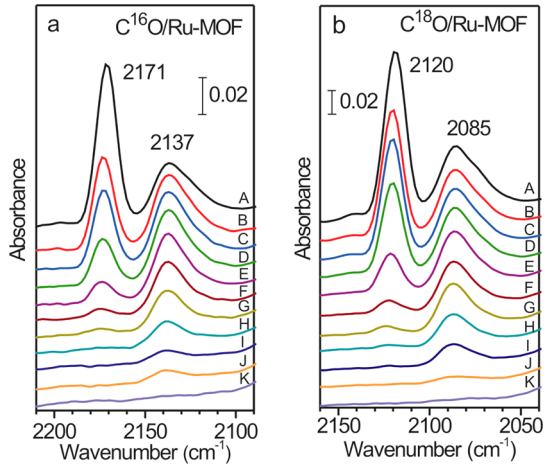

Figure 7. Thermal desorption of CO from **Ru-MOF** at 100–190 K. UHV-FTIR spectra obtained after exposing the clean **Ru-MOF** to (a) $C^{16}O$ and (b) $C^{18}O$ at 90 K (see Figure 5) and then heating to elevated temperatures: (A) exposure to $C^{16}O/C^{18}O$ (5×10^{-4} mbar) at 90 K; and heated to (B) 100, (C) 110, (D) 120, (E) 130, (F) 140, (G) 150, (H) 160, (I) 170, (J) 180, and (K) 190 K.

to the polarization of the adsorbed CO molecule.[56,57] The interaction of CO with metal cations can also involve charge donation from the CO 5σ orbital to the empty orbitals of metal atoms. The σ donation from CO to the substrate will strengthen the internal C–O bond, thus causing a blue shift of the C–O band. When the metal atoms possess partially filled d orbitals, the charge back-donation to the CO 2π^* antibonding orbital can also occur, which weakens the C–O bond (red shift in frequency) and strengthens the interaction between CO and substrates. From the frequency shift and thermal stability of the two CO bands observed for **Ru-MOF**, it seems that we could give a straightforward assignment: the 2137 and 2171 cm^{-1} bands could be attributed to CO species adsorbed, respectively, at "free" Ru^{II} CUS and Ru^{III} site coordinated to an additional Cl^- counterion within the paddle-wheel unit. The additional contribution of charge back-donation from Ru^{II} to CO would explain the enhanced binding energy and the red shift of the 2137 cm^{-1} band, as reported for the mixed-valence Fe-containing MOF (MIL-100).[13] However, this assignment is not supported by our accurate DFT calculations, which reveal that the interaction of CO with **Ru-MOF** is of a rather complex nature, as discussed in detail in the DFT calculation paragraph below.

From the spectroscopic results, we can conclude that at least one of the two different CO species should be due to a direct coordination to a CUS. However, no atomistic picture can be directly and unambiguously derived from the measured IR frequencies. Consequently, we have used theoretical first-principles DFT level calculations of nonperiodic model systems of the CUS to investigate various scenarios (Table 1, model structures **1**–**10**). Our benzoate model contains one carboxylate paddle-wheel unit with four phenyl groups (**1**), representing the aromatic backbone of the btc linker. Note that this size of model system is also successfully used in first-principles force field parametrization of such HKUST-1 analogous systems.[41] This includes both electronic effects of the aromatic carboxylate on the electron density at the transition-metal atoms as well as dispersive interactions between CO and the MOF framework, and represents a model system as close as possible to the true environment within the periodic **Ru-MOF** matrix. As discussed before, the straightforward model is used to envision a scenario with the mixed-valence $Ru_2^{II,III}$ as a starting point, and to coordinate one CO at the CUS, leading to **2** (Figure 8). In Table 1, all relevant

Table 1. Computed CO Binding Energies E_b and (Scaled) CO Vibrational Frequencies ν(C–O) for the Cluster Models Shown in Figure 8

		E_b [kJ/mol]	reference species for CO binding	ν(C–O) [cm^{-1}]	scaled ν(C–O) [cm^{-1}]
CO				2199.0	2143.0
1	Ru^{II}–$Ru^{III}Cl$				
2	OC–Ru^{II}–$Ru^{III}Cl$	121.9	**1**	2110.9	2057.1
3	OC–Ru^{II}–$Ru^{III}Cl$/CO	23.1	**2**	2111.6	2057.7
				2193.4	2137.5
4	OC–Ru^{II}–Ru^{III}–COCl	32.0	**2**	1935.2	1885.9
				2088.7	2035.4
5	$[Cl–Ru^{II}–Ru^{III}–Cl]^-$				
6	$[Ru^{II}–Ru^{III}]^+$				
7	$[Ru^{II}–Ru^{III}–CO]^+$	121.3	**6**	2155.5	2100.5
8	$[OC–Ru^{II}–Ru^{III}–CO]^+$	39.8	**7**	2150.4/2213.7	2095.6/2157.3
9	Ru^{II}–Ru^{II}–CO	133.7	Ru^{II}–Ru^{II}	2051.0	1998.7
10	$[OC–Ru^{III}–Ru^{III}–Cl]^+$	55.1	$[Ru^{III}–Ru^{III}–Cl]^+$	2167.3	2112.0

dx.doi.org/10.1021/jp3056366 | J. Phys. Chem. C 2013, 117, 5658–5666

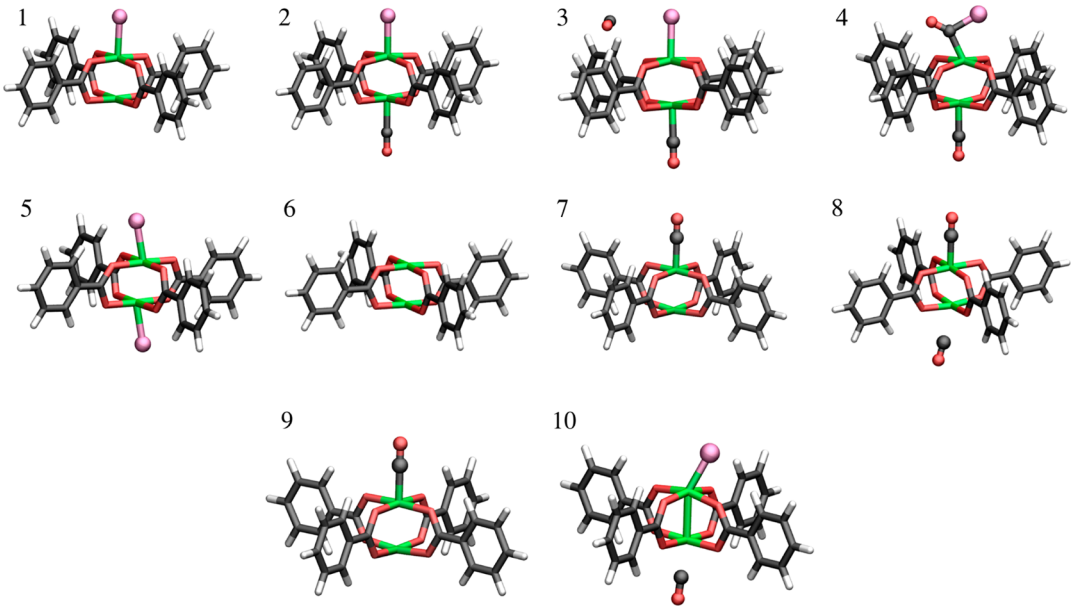

Figure 8. Computed model systems of CO adsorption for different scenarios of Cl and CO coordinated benzoate Ru dimer paddle-wheel systems as models for local structures of **Ru-MOF** (atom coloring: ruthenium, green; chlorine, magenta; carbon, black; oxygen, red; hydrogen, white).

relative energies of the computed species and the corresponding (scaled and unscaled) vibrational frequencies of CO in these systems are given. Note that the Ru atom exposing the CUS is expected to be the more electron-rich atom in the formal oxidation state II. This is reflected by the rather strong binding energy of about 120 kJ/mol and a reduction of the CO stretching vibration by about 90 cm^{-1} due to the electron back-donation into the π^* orbital of CO. DFT computed normal modes with appropriate scaling are known to be quite accurate and allow an assignment of measured IR bands.[58] The computed normal mode is substantially lower than both the experimentally determined bands, which, to our surprise, excludes this scenario for an explanation of the experimental observations. A higher frequency could be expected for the less electron-rich Ru^{III} site, and thus we investigated the coordination of a further CO on the Ru-Cl side. However, a dispersion-stabilized physisorbed precomplex is found in this case (**3**) and, only after passing a barrier, the second CO is bonded (**4**). Both structure and vibrational modes of **4** indicate that this is not a Ru−CO complex, but the CO has inserted into the Ru−Cl bond and a formylchloride is formed. In other words, a Cl^- ligand is replaced by a $[C(Cl)=O]^-$ fragment. This process is with about 30 kJ/mol only weakly exothermic, and the vibrational frequency of the second formylchloride CO stretch is with 1885 cm^{-1} even lower than the Ru^{II} bound CO. Because of this, the insertion into the Ru−Cl bond can also be excluded, not just from energetic reasons. Note that a formylchloride formation without prior CO coordination on the Ru^{II} CUS can be excluded for energetic reasons. Thus, any scenario of a CO coordination to the "native" $Ru_2^{II,III}$ fragment does not lead to a match between theoretically computed and measured vibrational modes.

As a consequence, we have extended our theoretical investigations to further scenarios. There is, in principle, one avenue to form a CUS with an exposed Ru^{III} atom without invoking a redox process. If one of the Cl^- counterions is transferred to a neighboring CUS, the overall mixed-valence state of $Ru_2^{II,III}$ would be maintained. By this process, one negatively charged paddle-wheel unit would be completely blocked by Cl (**5**), whereas the other positively charged Ru dimer (**6**) exposes now two CUS together with the $Ru_2^{II,III}$ nature of each unit being maintained. In the gas phase, this process leading from two **1** to **5** and **6** is only 120 kJ/mol uphill in energy. In the periodic framework, such a chloride transfer is likely to be additionally stabilized by long-range electrostatic interactions. As a result, the bare cationic system **6** can now coordinate two CO ligands, leading to **7** and **8**. The first CO binds with a similar binding energy as to the chloride coordinated **1** (about 120 kJ/mol), but the reduced electron density for the cationic system results in a somewhat higher vibrational mode of about 2100 cm^{-1}. The second CO binds much weaker on the other side with about 40 kJ/mol, resulting in a second IR absorption around 2160 cm^{-1}. Overall, this second model fits much better with the experimental observations, since two vibrational modes in the right range are computed, with the higher one being more weakly bonded. It is also consistent with XPS results, indicating a mixed-valence state. Note that, by removing the coordinated chloride and solvating it somewhere in the pore, a similar CO bonding would result. However, in such a case, the observed Ru−Cl IR band (see Figure 4) cannot be explained. Nevertheless, this scenario is built on the assumption of a chloride transfer, which is, at least in the gas phase, endothermic.

A further alternative is to assume redox processes taking place under **Ru-MOF** growth conditions. To complete the picture, we investigated both a reduction of the mixed-valence state, leading to a Ru(II)-Ru(II) paddle-wheel. In this case, the counterion is removed, which leads essentially to a neutral paddle-wheel identical to the parent copper-based HKUST-1. Since the redox process itself is unknown, we cannot assess the thermodynamic stability of these species. Thus, we focus here just on a comparison of the CO binding energies and the resulting IR stretching modes. As expected for a Ru(II) system with a stronger back-bonding interaction, a strong binding energy of 134 kJ/mol is computed, and also a low CO stretch mode of 1999 cm^{-1} is predicted (**9**). We included this reduced system only for completeness, but we can rule out its presence in the actual system. On the other hand, in principle, an

dx.doi.org/10.1021/jp3056366 | J. Phys. Chem. C 2013, 117, 5658−5666

oxidation of the second Ru would result in a Ru(III)-Ru(III)-Cl type cationic dimer. Again, some charge-balancing counterion must be assumed. In this case, CO binds with only 55 kJ/mol and a CO band at 2112 cm^{-1} is found (**10**). This result is much better in line with the measured vibrational modes, but cannot explain the two distinct CO modes. In addition, the different charge state of the metal atoms observed in XPS is not consistent with this picture.

At this point, we can only conclude that the atomistic picture of **Ru-MOF** is, in fact, much more complex than expected. In particular, a straightforward CO coordination to the chloride coordinated mixed-valence paddle-wheel does not lead to computed normal modes, in good agreement with the experimental results. The best match is found for a scenario, where a chloride is redox-neutrally transferred to a neighboring paddle-wheel, leading to a charge separation and alternating cationic and anionic SBUs. This scenario is, however, a pure hypothesis at the current stage, and further experimental and theoretical investigations beyond the scope of the current work will have to be performed to fully clarify this situation.

CONCLUSIONS

The mixed-valence metal−organic framework $[Ru_3^{II,III}(btc)_2Cl_{1.5}]$ (**Ru-MOF**) was prepared by the controlled SBU approach using $[Ru_2^{II,III}(OOCCH_3)_4Cl]$ as a precursor. The high-quality IR data obtained after CO adsorption on **Ru-MOF** at 90 K reveal the presence of two kinds of CO species bound to Ru cation sites within the framework after activation of the sample under UHV conditions. The 2171 cm^{-1} band is attributed to a weakly bonded CO species, whereas the low-lying CO band at 2137 cm^{-1} originates from CO species with an enhanced binding energy. On the basis of the DFT calculations with respect to a number of possible scenarios of CO/Cl coordination, we demonstrate that the two IR bands *cannot* be assigned in a straightforward manner to CO species bound to "free" Ru^{II} CUS (2137 cm^{-1}) and Ru^{III} connected to a Cl^- counterion (2171 cm^{-1}). In contrast, the structural and electronic properties of mixed-valence **Ru-MOF** are much more complex than expected. A possible assignment, leading to the best match between DFT calculations on model systems and experimental data, is based on the assumption that one of the Cl^- counterions is transferred to a neighboring paddle-wheel, leading to the formation of an anionic SBU in which potential CUS are blocked by two Cl^- ions. As a consequence, the other positively charged paddle-wheel with a $Ru_2^{II,III}$ dimer exposes two CUS, where two different Ru-CO species can be formed, as confirmed by the IR data. Further experimental and theoretical studies are required for a thorough understanding of the interaction between CO and mixed-valence MOFs.

In this context, it needs to be recognized that the discussed complexity is by no means a singularity for this particular case. Rather, the multivariate scenario is intimately connected to the mixed-valence state of the respective paddle-wheel building unit (maybe for all oligo/multimetal ion building units), the possible need for charge compensation, and the possibility of transfer of coordinative noninnocent counterions between metal ion sites of the framework. Thus, we conclude that a similar complexity needs to be taken into explicit account for many other mixed-valence MOFs with intrinsically (coordinative) open metal sites (CUS), which, however, is not usually done in accurate detail so far.[59−63] Within a porous crystalline coordination network material, not only MOFs, it is hard to establish the actual atomistic structure and electronic configuration of the metal ion framework sites by experimental techniques, since local probes are needed, whereas diffraction-based methods are not helpful as these give average information (of translational periodicity), only. To our knowledge, our study is one of the very few combining highly accurate UHV-FTIR spectroscopy with DFT calculations for assignment and discussion of the observed IR data of probe molecule (CO, etc.) adsorption to CUS in MOFs.[64] Our results reveal that a conclusive answer about the actual state of the MOF (and thus its potential and rationalization, e.g., for catalytic reactions) can be much more difficult to find in general, as one would (naively) expect. On the other hand, we want to point out that this interesting complexity is not just a problem of spectroscopic assignment. It rather could hold much potential for new and interesting properties of mixed-valence MOFs and MOFs in general with a higher degree of compositional variations but exhibiting the same overall framework structure and topology.

AUTHOR INFORMATION

Corresponding Author

*Tel: +49-234-3224166 (R.S.), +49-234-3224174 (R.A.F.), +49-234-3224217 (Y.W.). Fax: +49-234-3214174 (R.S.), +49-234-3214174 (R.A.F.), +49 234 3214184 (Y.W.). E-mail: rochus.schmid@rub.de (R.S.), roland.fischer@rub.de (R.A.F.), wang@pc.rub.de (Y.W.).

Present Address

[+]Deutsches Elektronen-Synchrotron DESY, Notkerstrasse 85, 22607 Hamburg, Germany.

Notes

The authors declare no competing financial interest.

ACKNOWLEDGMENTS

This work was supported by the German Research Foundation (DFG) through the Research Centre SFB558 "Metal-Substrate Interactions in Heterogeneous Catalysis". O.K. thanks the Ruhr University Research School at Bochum for a Ph.D. grant (www.research-school.rub.de). H.N. and M.K. carried out the UHV-FTIRS and XPS measurements. O.K. synthesized, activated, and analytically characterized the samples. B.M. supported the work by supply of far-IR data. S.A. and S.B. performed the DFT calculations and R.S. supervised this part of the joint project. M.M and, in particular, Y.W. directed the work packages related to the UHV-FTIR and XPS studies. R.A.F supervised the involved coordination chemistry and was responsible for overall guiding this collaborative work.

REFERENCES

(1) Yaghi, O. M.; O'Keeffe, M.; Ockwig, N. W.; Chae, H. K.; Eddaoudi, M.; Kim, J. Reticular Synthesis and the Design of New Materials. *Nature* **2003**, *423*, 705−714.

(2) Kitagawa, S.; Matsuda, R. Chemistry of Coordination Space of Porous Coordination Polymers. *Coord. Chem. Rev.* **2007**, *251*, 2490−2509.

(3) Wang, Z.; Tanabe, K. K.; Cohen, S. M. Accessing Postsynthetic Modification in a Series of Metal−Organic Frameworks and the Influence of Framework Topology on Reactivity. *Inorg. Chem.* **2009**, *48*, 296−306.

(4) Tanabe, K. K.; Cohen, S. M. Postsynthetic Modification of Metal−Organic Frameworks—A Progress Report. *Chem. Soc. Rev.* **2011**, *40*, 498−519.

(5) Kim, H.; Chun, H.; Kim, K.; Collins, D. J.; Ma, Sh.; Zhou, H.-C. *Metal-Organic Frameworks: Designing and Application*; MacGillivray, L. R., Ed.; John Wiley & Sons, Inc.: Hoboken, NJ, 2010; Parts 7 and 8, pp 215−267.

(6) Achmann, S.; Hagen, G.; Kita, J.; Malkowsky, I. M.; Kiener, Ch.; Moos, R. Metal-Organic Frameworks for Sensing Applications in the Gas Phase. *Sensors* **2009**, *9*, 1574−1589.
(7) Lee, J. Y.; Farha, O. K.; Roberts, J.; Scheidt, K. A.; Nguyen, S. T.; Hupp, J. T. Metal−Organic Framework Materials as Catalysts. *Chem. Soc. Rev.* **2009**, *38*, 1450−1459.
(8) Ranocchiari, M.; Van Bokhoven, J. A. Catalysis by Metal−Organic Frameworks: Fundamentals and Opportunities. *Phys. Chem. Chem. Phys.* **2011**, *13*, 6388−6396.
(9) Horcajada, P.; Serre, Ch.; Maurin, G.; Ramsahye, N. A.; Balas, F.; Vallet-Regi, M.; Sebban, F.; Taulelle, M.; Férey, G. Flexible Porous Metal−Organic Frameworks for a Controlled Drug Delivery. *J. Am. Chem. Soc.* **2008**, *130*, 6774−6780.
(10) Huxford, R. C.; Della Rocca, J.; Lin, W. Metal−Organic Frameworks as Potential Drug Carriers. *Curr. Opin. Chem. Biol.* **2010**, *14*, 262−268.
(11) Burrows, A. D. Mixed-Component Metal−Organic Frameworks (MC-MOFs): Enhancing Functionality Through Solid Solution Formation and Surface Modifications. *CrystEngComm* **2011**, *13*, 3623−3642.
(12) Férey, G.; Millange, F.; Morcrette, M.; Serre, C.; Doublet, M.-L.; Grenèche, J.-M.; Tarascon, J.-M. Mixed-Valence Li/Fe-Based Metal−-Organic Frameworks with Both Reversible Redox and Sorption Properties. *Angew. Chem., Int. Ed.* **2007**, *46*, 3259−3263.
(13) Yoon, J. W.; Seo, Y. K.; Hwang, Y. K.; Chang, J. S.; Leclerc, H.; Wuttke, S.; Bazin, P.; Vimont, A.; Daturi, M.; Bloch, E.; et al. Controlled Reducibility of a Metal−Organic Framework with Coordinatively Unsaturated Sites for Preferential Gas Sorption. *Angew. Chem., Int. Ed.* **2010**, *49*, 5949−5952.
(14) He, J.; Zhang, J.-X.; Tsang, Ch.-K.; Xu, Zh.; Yin, Y.-G.; Li, D.; Ng, S.-W. Mixed-Valence $Cu(II)Cu(I)_{15}I_{17}$ Cluster Builds up a 3D Metal−Organic Framework with Paramagnetic and Thermochromic Characteristics. *Inorg. Chem.* **2008**, *47*, 7948−7950.
(15) Combelles, C.; Doublet, M.-L. Structural, Magnetic and Redox Properties of a New Cathode Material for Li-Ion Batteries: The Iron-Based Metal Organic Framework. *Ionics* **2008**, *14*, 279−283.
(16) Medina, M. E.; Dumont, Y.; Grenèche, J.-M.; Millange, F. Fe(III)/Fe(II) Regular Charge Order in Metal−Organic Framework. *Chem. Commun.* **2010**, *46*, 7987−7989.
(17) Combelles, C.; Ben Yahia, M.; Pedesseau, L.; Doublet, M.-L. Design of Electrode Materials for Lithium-Ion Batteries: The Example of Metal−Organic Framework. *J. Phys. Chem. C* **2010**, *114*, 9518−9527.
(18) Combelles, C.; Ben Yahia, M.; Pedesseau, L.; Doublet, M.-L. FeII/FeIII Mixed-Valence State Induced by Li-Insertion into the Metal-Organic-Framework Mil53(Fe): A DFT+U Study. *J. Power Sources* **2011**, *196*, 3426−3432.
(19) Takaishi, S.; Hosoda, M.; Kajiwara, T.; Miyasaka, H.; Yamashita, M.; Nakanishi, Y.; Kitagawa, Y.; Yamaguchi, K.; Kobayashi, A.; Kitagawa, H. Electroconductive Porous Coordination Polymer $Cu-[Cu(pdt)_2]$ Composed of Donor and Acceptor Building Units. *Inorg. Chem.* **2009**, *48*, 9048−9050.
(20) Kobayashi, Y.; Jacobs, B.; Allendorf, M. D.; Long, J. R. Conductivity, Doping, and Redox Chemistry of a Microporous Dithiolene-Based Metal−Organic Framework. *Chem. Mater.* **2010**, *22*, 4120−4122.
(21) Noei, H.; Amirjalayer, S.; Müller, M.; Zhang, X.; Schmid, R.; Muhler, M.; Fischer, R. A.; Wang, Y. Low-Temperature CO Oxidation over Cu-Based Metal−Organic Frameworks Monitored by Using FTIR Spectroscopy. *ChemCatChem* **2012**, *4*, 755−759.
(22) Kozachuk, O.; Yusenko, K.; Noei, H.; Wang, Y.; Walleck, S.; Glaser, T.; Fischer, R. A. Solvothermal Growth of a Ruthenium Metal−Organic Framework Featuring HKUST-1 Structure Type as Thin Films on Oxide Surfaces. *Chem. Commun.* **2011**, *47*, 8509−8511.
(23) Chui, S. S. Y.; Lo, S. M. F.; Charmant, J. P. H.; Orpen, A. G.; Williams, I. D. A Chemically Functionalizable Nanoporous Material $[Cu_3(TMA)_2(H_2O)_3]_n$. *Science* **1999**, *283*, 1148−1150.
(24) Köberl, M.; Cokoja, M.; Herrmann, W. A.; Kühn, F. E. From Molecules to Materials: Molecular Paddle-Wheel Synthons of Macromolecules, Cage Compounds and Metal−Organic Frameworks. *Dalton Trans.* **2011**, *40*, 6834−6859.
(25) Kramer, M.; Schwarz, U.; Kaskel, S. Synthesis and Properties of The Metal-Organic Framework $Mo_3(BTC)_2$ (TUDMOF-1). *J. Mater. Chem.* **2006**, *16*, 2245−2248.
(26) Murray, L. J.; Dinca, M.; Yano, J.; Chavan, S.; Bordiga, S.; Brown, C. M.; Long, J. R. Highly-Selective and Reversible O_2 Binding in Cr_3(1,3,5-Benzenetricarboxylate)$_2$. *J. Am. Chem. Soc.* **2010**, *132*, 7856−7857.
(27) Feldblyum, J. I.; Liu, M.; Gidley, D. W.; Matzger, A. J. Reconciling the Discrepancies between Crystallographic Porosity and Guest Access As Exemplified by Zn-HKUST-1. *J. Am. Chem. Soc.* **2011**, *133*, 18257−18263.
(28) Wang, Y.; Glenz, A.; Muhler, M.; Wöll, C. A New Dual-Purpose Ultrahigh Vacuum Infrared Spectroscopy Apparatus Optimized for Grazing-Incidence Reflection as Well as for Transmission Geometries. *Rev. Sci. Instrum.* **2009**, *80*, 113108.
(29) Lamberti, C.; Zecchina, A.; Groppo, E.; Bordiga, S. Probing the Surfaces of Heterogeneous Catalysts by in Situ IR Spectroscopy. *Chem. Soc. Rev.* **2010**, *39*, 4951−5001.
(30) Garrone, E.; Otero-Arean, C. Variable Temperature Infrared Spectroscopy: A Convenient Tool for Studying the Thermodynamics of Weak Solid−Gas Interactions. *Chem. Soc. Rev.* **2005**, *34*, 846−857.
(31) Esken, D.; Noei, H.; Wang, Y.; Wiktor, C.; Turner, S.; Van Tendeloo, G.; Fischer, R. A. ZnO@ZIF-8: Stabilization of Quantum Confined ZnO Nanoparticles by a Zinc Methylimidazolate Framework and Their Surface Structural Characterization Probed by CO_2 Adsorption. *J. Mater. Chem.* **2011**, *21*, 5907−5915.
(32) Mitchell, R. W.; Spenser, A.; Wilkinson, G. Carboxylato-Triphenylphosphine Complexes of Ruthenium, Cationic Triphenylphosphine Complexes Derived from Them, and Their Behaviour as Homogeneous Hydrogenation Catalysts for Alkenes. *J. Chem. Soc., Dalton Trans.* **1973**, 846−854.
(33) *TURBOMOLE V6.3*; **2011**. A development of University of Karlsruhe and Forschungszentrum Karlsruhe GmbH, 1989−2007, TURBOMOLE GmbH, since 2007. Available from http://www.turbomole.com.
(34) Becke, A. D. Density-Functional Exchange-Energy Approximation with Correct Asymptotic Behavior. *Phys. Rev. A* **1988**, *38*, 3098−3100.
(35) Becke, A. D. Density-Functional Thermochemistry. III. The Role of Exact Exchange. *J. Chem. Phys.* **1993**, *98*, 5648−5652.
(36) Lee, C.; Yang, W.; Parr, R. G. Development of the Colle-Salvetti Correlation-Energy Formula into a Functional of the Electron Density. *Phys. Rev. B* **1988**, *37*, 785−789.
(37) Stephens, P. J.; Devlin, F. J.; Chabalowski, C. F.; Frisch, M. J. *Ab Initio* Calculation of Vibrational Absorption and Circular Dichroism Spectra Using Density Functional Force Fields. *J. Phys. Chem.* **1994**, *98*, 11623−11627.
(38) Dunning, T. H. Gaussian Basis Sets for Use in Correlated Molecular Calculations. I. The Atoms Boron Through Neon and Hydrogen. *J. Chem. Phys.* **1989**, *90*, 1007−1023.
(39) Peterson, K. A.; Figgen, D.; Dolg, M.; Stoll, H. Energy-Consistent Relativistic Pseudopotentials and Correlation Consistent Basis Sets for the 4*d* Elements Y−Pd. *J. Chem. Phys.* **2007**, *126*, 124101−124112.
(40) Grimme, S.; Antony, J.; Ehrlich, S.; Krieg, H. A Consistent and Accurate *ab Initio* Parametrization of Density Functional Dispersion Correction (DFT-D) for the 94 Elements H-Pu. *J. Chem. Phys.* **2010**, *132*, 154104.
(41) Bureekaew, S.; Amirjalayer, S.; Tafipolsky, M.; Spickermann, C.; Roy, T. K.; Schmid, R. MOF-FF − A Flexible First Principles Derived Force Field for Metal-Organic Frameworks. *Phys. Status Solidi B* **2013**, DOI: 10.1002/pssb.201248460.
(42) Zaki, M. I.; Knözinger, H. An Infrared Spectroscopy Study of Carbon Monoxide Adsorption on α-Chromia Surfaces: Probing Oxidation States of Coordinatively Unsaturated Surface Cations. *J. Catal.* **1989**, *119*, 311−321.

(43) Kim, J.; Chen, B.; Reineke, T. M.; Li, H.; Eddaoudi, M.; Moler, D. B.; ÓKeeffe, M.; Yaghi, O. M. Assembly of Metal−Organic Frameworks from Large Organic and Inorganic Secondary Building Units: New Examples and Simplifying Principles for Complex Structures. *J. Am. Chem. Soc.* **2001**, *123*, 8239−8247.
(44) Yaghi, O. M.; ÓKeeffe, M.; Ockwig, N. W.; Chae, H. K.; Eddaoudi, M.; Kim, J. Reticular Synthesis and the Design of New Materials. *Nature* **2003**, *423*, 705−714.
(45) Togano, T.; Mukaida, M.; Nomura, T. The Crystal Structure of Tetra-μ-acetato-diruthenium Chloride. *Bull. Chem. Soc. Jpn.* **1980**, *53*, 2085−2086.
(46) Aquino, M. A. S. Diruthenium and Diosmium Tetracarboxylates: Synthesis, Physical Properties and Applications. *Coord. Chem. Rev.* **1998**, *170*, 141−202.
(47) Moulder, J. F.; Stickle, W. F.; Sobol, P. E.; Bomben, K. D. *Handbook of X-Ray Photoelectron Spectroscopy*; Perkin-Elmer Corporation, Physical Electronics Division: Eden Prairie, MN, 1992.
(48) Ivanovskaya, M. I.; Romanovskaya, V. V.; Branitsky, G. A Composite Materials Based on Ti and Ru Oxides. *J. Mater. Chem.* **1994**, *4*, 373−377.
(49) Xie, L.; Liu, S.; Gao, C.; Cao, R.; Cao, J.; Sun, C.; Su, Z. Mixed-Valence Iron(II, III) Trimesates with Open Frameworks Modulated by Solvents. *Inorg. Chem.* **2007**, *46*, 7782−7788.
(50) Bennett, M. J.; Caulton, K. G.; Cotton, F. A. Structure of Tetra-*n*-Butyratodiruthenium Chloride, a Compound with a Strong Metal−Metal Bond. *Inorg. Chem.* **1969**, *8*, 1−6.
(51) Bino, A.; Cotton, F. A.; Felthouse, T. R. Structural Studies of Some Multiply Bonded Diruthenium Tetracarboxylate Compounds. *Inorg. Chem.* **1979**, *18*, 2599−2604.
(52) Barral, M. C.; Jimenez-Aparicio, R.; Royer, E. C.; Ruiz-Valero, C.; Saucedo, M. J.; Urbanos, F. A. Synthesis and X-ray Structure of the First Nonpolymeric Chlorotetrakis(carboxylato)diruthenium(II,III) Compound. *Inorg. Chem.* **1994**, *33*, 2692−2694.
(53) Takamizawa, S.; Yamaguchi, K.; Mori, W. The Gas-Occlusion Properties of Dicarboxylate (Fumarate, *trans-trans*-Muconate and Terephthalate) Ruthenium(II,III) Dinuclear Complexes. *Inorg. Chem. Commun.* **1998**, *1*, 177−178.
(54) Barral, M. C.; Gonzalez-Prieto, R.; Jimenez-Aparicio, R.; Priego, J. L.; Torres, M. R.; Urbanos, F. A. Polymeric, Molecular, and Cation/Anion Arrangements in Chloro-, Bromo-, and Iododiruthenium(II,III) Carboxylate Compounds. *Eur. J. Inorg. Chem.* **2003**, 2339−2347.
(55) Cotton, S. A. *Chemistry of Precious Metals*; Chapman & Hall: London, 1997.
(56) Zecchina, A.; Otero Arean, C. Diatomic Molecular Probes for Mid-IR Studies of Zeolite. *Chem. Soc. Rev.* **1996**, *25*, 187−197.
(57) Pacchioni, G.; Ferrari, A. M.; Bagus, P, S. Cluster and Band Structure Ab Initio Calculations on the Adsorption of CO on Acid Sites of the TiO_2(110) Surface. *Surf. Sci.* **1996**, *350*, 159−175.
(58) Xu, M.; Noei, H.; Fink, K.; Muhler, M.; Wang, Y.; Wöll, C. The Surface Science Approach for Understanding Reactions on Oxide Powders: The Importance of IR Spectroscopy. *Angew. Chem., Int. Ed.* **2012**, *51*, 4731−4734.
(59) Bordiga, S.; Regli, L.; Bonino, F.; Groppo, E.; Lamberti, C.; Xiao, B.; Wheatley, P. S.; Morris, R. E.; Zecchina, A. Adsorption Properties of HKUST-1 Toward Hydrogen and Other Small Molecules Monitored by IR. *Phys. Chem. Chem. Phys.* **2007**, *9*, 2676−2685.
(60) Alaerts, L.; Seguin, E.; Poelman, H.; Thibault-Starzyk, F.; Jacobs, P. A.; De Vos, D. E. Probing the Lewis Acidity and Catalytic Activity of the Metal−Organic Framework $[Cu_3(btc)_2]$ (BTC = Benzene-1,3,5-tricarboxylate). *Chem.—Eur. J.* **2006**, *12*, 7353−7363.
(61) Leclerc, H.; Vimont, A.; Lavalley, J. C.; Daturi, M.; Wiersum, A. D.; Llwellyn, P. L.; Horcajada, P.; Ferey, G.; Serre, C. Infrared Study of the Influence of Reducible Iron(III) Metal Sites on the Adsorption of CO, CO_2, Propane, Propene and Propyne in the Mesoporous Metal−Organic Framework MIL-100. *Phys. Chem. Chem. Phys.* **2011**, *13*, 11748−11756.
(62) Hwang, Y. K.; Hong, D. Y.; Chang, J. S.; Jhung, S. H.; Seo, Y. K.; Kim, J.; Vimont, A.; Daturi, M.; Serre, C.; Ferey, G. Amine Grafting on Coordinatively Unsaturated Metal Centers of MOFs: Consequences for Catalysis and Metal Encapsulation. *Angew. Chem., Int. Ed.* **2008**, *47*, 4144−4148.
(63) Vimont, A.; Leclerc, H.; Mauge, F.; Daturi, M.; Lavalley, J. C.; Surble, S.; Serre, C.; Ferey, G. Creation of Controlled Brønsted Acidity on a Zeotypic Mesoporous Chromium(III) Carboxylate by Grafting Water and Alcohol Molecules. *J. Phys. Chem. C* **2007**, *111*, 383−388.
(64) Valenzano, L.; Vitillo, J. G.; Chavan, S.; Civalleri, B.; Bonino, F.; Bordiga, S.; Lamberti, C. Structure—Activity Relationships of Simple Molecules Adsorbed on CPO-27-Ni Metal—Organic Framework: In situ Experiments vs. Theory. *Catal. Today* **2012**, *182*, 67−79.